

Parameterisation of radiation forces for a multiple degree-of-freedom wave energy converter using moment-matching

Original

Parameterisation of radiation forces for a multiple degree-of-freedom wave energy converter using moment-matching / Faedo, N.; Pena-Sanchez, Y.; Ringwood, J. V.. - 1:(2019), pp. 166-173. (Intervento presentato al convegno 29th International Offshore and Polar Engineering Conference (ISOPE 2019)).

Availability:

This version is available at: 11583/2988079 since: 2024-04-24T12:33:55Z

Publisher:

INTERNATIONAL SOCIETY OF OFFSHORE AND POLAR ENGINEERING

Published

DOI:

Terms of use:

This article is made available under terms and conditions as specified in the corresponding bibliographic description in the repository

Publisher copyright

(Article begins on next page)

Parameterisation of Radiation Forces for Multiple Degree-of-Freedom Wave Energy Converters Using Moment-Matching

Nicolás Faedo, Yerai Peña-Sanchez and John V. Ringwood
Centre for Ocean Energy Research, Maynooth University
Maynooth, Ireland

The motion of a wave energy converter (WEC) can be described in terms of an integro-differential equation, which involves a convolution operator. This convolution term accounts for the effect of radiation forces acting on the device and represents a computational and representational drawback both for simulation and analysis/design of control/estimation strategies. We present herein a moment-based strategy to compute a parametric form of the radiation force subsystem for multiple degree-of-freedom WECs. The strategy allows for the computation of a model that exactly matches the steady-state behaviour of the target system at a set of user-defined frequencies, while retaining the underlying physical properties of radiation forces. The potential and capabilities of the presented method are illustrated considering a CorPower-like device (heaving point absorber) as an application case.

INTRODUCTION

Among the different modelling approaches adopted in the wave energy literature (see Li and Yu, 2012), the speed with which numerical simulation may be performed makes the widely known boundary element method (BEM) a common choice to compute hydrodynamic parameters for a given wave energy converter (WEC) (Penalba et al., 2017). However, one of the major drawbacks of the BEM is that the results are computed in the frequency domain and, hence, can only characterise the steady-state motion of the WEC under analysis. Seeking a more comprehensive approach and following the well-known theory developed in Cummins (1962), the motion of a WEC can be expressed, in the time domain, using a particular well-known integro-differential equation of the convolution class. The presence of these convolution terms accounts for the effect of radiation forces acting on each of the different degrees of freedom (DoF) of the device, constituting a (hydrodynamic) coupling between these modes of motion.

The existence of these convolution terms represents a significant drawback both for motion simulation and for modern analysis/design of control/estimation strategies. From a motion simulation point of view, it is well known that the explicit computation of the convolution operator is computationally inefficient, often worsened by the necessity of a small (time) discretisation step to obtain accurate numerical integration. From a control/estimation theory point of view, the presence of these convolution mappings complicates the application of well-established results in the field, since modern control/estimation techniques are based on the availability of a state-space representation (at least in local coordinates) of the system under analysis (Faedo et al., 2017). Motivated by these drawbacks, researchers often seek for a parametric approximation of this radiation force subsystem in terms of a linear time-invariant dynamic representation, making explicit use

of the corresponding hydrodynamic characteristics of the device obtained from BEM solvers.

To be precise, the prevailing approach is to approximate each convolution term independently (see, for example, Pérez and Fossen (2008) and Giorgi and Ringwood (2019), as a single-input single-output (SISO) dynamic system, although the problem is inherently multiple-input multiple-output (MIMO), as a consequence of the multi-DoF characteristic of the WEC. One main disadvantage of this “multi-SISO” approach is that treating each convolution term independently often leads to an unnecessary high-order dimensional parameterisation of the radiation force subsystem, potentially rendering any control/estimation strategy challenging for real-time applications (Faedo et al., 2017).

We have recently presented a moment-matching-based MIMO identification method for wave energy applications in Faedo et al. (2019), particularly to approximate the response of an array of WECs, i.e. a “farm” of multiple 1-DoF devices. This strategy is based on the underlying theoretical concepts developed in Faedo et al. (2018b), and it allows for the computation of a model that exactly matches the frequency response of the target MIMO system at a set of user-selected frequencies \mathcal{F} , providing an efficient and accurate method to compute a state-space representation for the WEC dynamics. Additionally, a wise selection of the set \mathcal{F} within this moment-based approach helps to enforce the underlying (physical) properties of the WEC under analysis.

Motivated by these results, in this paper we present an adaptation of the MIMO identification framework developed in Faedo et al. (2019) to compute a parametric approximation of the radiation force subsystem of a multi-DoF device. We demonstrate that treating the approximation of radiation forces with our MIMO moment-based strategy (instead of the usual “multi-SISO” approach) provides a highly accurate low-dimensional system, hence offering a reliable parametric model while also reducing the computational effort required for time-domain simulations and control/estimation calculations. Moreover, we show that we can guarantee physical properties of radiation forces in the approximating model, such as bounded-input bounded-output (BIBO) stability.

The remainder of this paper is organised as follows. The section titled “Moments for MIMO Systems” recalls the theory behind moment-matching for MIMO systems. The section titled

Received July 18, 2019; updated and further revised manuscript received by the editors December 30, 2019. The original version (prior to the final updated and revised manuscript) was presented at the Twentieth International Ocean and Polar Engineering Conference (ISOPE-2019), Honolulu, Hawaii, June 16–21, 2019.

KEY WORDS: Radiation forces, parametric form, model order reduction, frequency-domain identification, moment-matching.

“Equations of Motion for a Multi-DoF WEC” briefly discusses modelling of multi-DoF WECs in both the time and frequency domains. The section titled “Moment-Based Radiation System” presents a moment-domain analysis of radiation forces, while the section titled “Models Achieving Moment-Matching” discusses a moment-based algorithm to compute a parametric approximation for the radiation force subsystem of a multi-DoF WEC. The section “Application to a Corporate-like Device” discusses an application case, where a CorPower-like device (see Fig. 1a) is considered. Finally, “Conclusions” encompasses the main conclusions of this study.

Notation and Preliminaries

Standard notation is considered through this study, with any exceptions detailed in this section. \mathbb{R}^+ (\mathbb{R}^-) denotes the set of non-negative (non-positive) real numbers. \mathbb{C}^0 denotes the set of pure-imaginary complex numbers, and $\mathbb{C}_{<0}$ denotes the set of complex numbers with a negative real part. The symbol 0 stands for any zero element, dimensioned according to the context. The symbol \mathbb{I}_n denotes an order n identity matrix. The spectrum of a matrix $A \in \mathbb{R}^{n \times n}$, i.e., the set of its eigenvalues, is denoted as $\lambda(A)$. The notation W^\dagger , with $W \in \mathbb{R}^{n \times m}$, denotes the Moore–Penrose inverse of W . The symbol $\bigoplus_{i=1}^n A_i$ denotes the direct sum of n matrices, i.e., $\bigoplus_{i=1}^n A_i = \text{diag}(A_1, A_2, \dots, A_n)$. The expression $\|X\|_F$ denotes the Frobenius norm of the matrix X . The Kronecker product between two matrices $M_1 \in \mathbb{R}^{n \times m}$ and $M_2 \in \mathbb{R}^{p \times q}$ is denoted as $M_1 \otimes M_2 \in \mathbb{R}^{np \times mq}$. The convolution between two functions f and g over a set $\Omega \subset \mathbb{R}$, i.e., $\int_{\Omega} f(\tau)g(t-\tau) d\tau$ is denoted as $f * g$. The Fourier transform of a function $f \in L^2(\mathbb{R})$ is denoted by $\mathcal{F}\{f(t)\} = \hat{f}(j\omega)$, while its Laplace transform is denoted as $\mathcal{L}\{f(t)\} = F(s)$, where $L^2(\mathbb{R}) = \{f : \mathbb{R} \rightarrow \mathbb{C} \mid \int_{\mathbb{R}} |f(t)|^2 dt < +\infty\}$. The notation $\Re\{z\}$ and $\Im\{z\}$ denote the real and imaginary parts of $z \in \mathbb{C}$. The symbol $e_{ij}^q \in \mathbb{R}^{q \times q}$ denotes a matrix with 1 in the ij component and 0 elsewhere. Finally, the symbol $\varepsilon_n \in \mathbb{R}^{n \times 1}$ denotes a vector with odd components equal to 1 and even components equal to 0.

MOMENTS FOR MIMO SYSTEMS

We note that the theory recalled herein is originated within the field of model order reduction in Astolfi (2010), being adapted for the WEC identification problem in Faedo et al. (2018b, 2019) and Peña-Sanchez et al. (2019b). The interested reader is referred to Scarciotti and Astolfi (2017, Chapter 1) for a thorough discussion on different model order reduction techniques and, particularly, on moment-based methods.

Consider a finite-dimensional, MIMO, continuous-time system Σ described, for $t \in \mathbb{R}^+$, by the state-space model

$$\Sigma : \{\dot{x}(t) = Ax(t) + Bu(t), y(t) = Cx(t)\} \quad (1)$$

with $x(t) \in \mathbb{R}^n$, $u(t) \in \mathbb{R}^q$, $y(t) \in \mathbb{R}^q$, $A \in \mathbb{R}^{n \times n}$, $B \in \mathbb{R}^{n \times q}$, and $C \in \mathbb{R}^{q \times n}$. Note that we focus on square systems, in line with the radiation force subsystem application. Consider the transfer function $W : \mathbb{C} \rightarrow \mathbb{C}^{q \times q}$, computed in terms of the associated impulse response matrix $w(t) = Ce^{At}B$ with $w_{ij} \in L^2(\mathbb{R})$, where w_{ij} denotes the ij element of w , as

$$\mathcal{L}\{w(t)\} \mapsto W(s) = C(s\mathbb{I}_n - A)^{-1}B \quad (2)$$

and assume that Eq. 1 is minimal, i.e., controllable and observable.

Definition 1 (Astolfi, 2010). The 0-moment of system Eq. 1 at $s_i \in \mathbb{C} \setminus \lambda(A)$ is the complex matrix $\eta_0(s_i) = C(s_i\mathbb{I}_n - A)^{-1}B$. The

k -moment of system Eq. 1 at $s_i \in \mathbb{C}$ is the complex matrix

$$\eta_k(s_i) = \frac{(-1)^k}{k!} \left[\frac{d^k}{ds^k} W(s) \right]_{s=s_i} \quad (3)$$

with $k \geq 1$ integer.

Remark 1. Note that moments, as in Definition 1, are the coefficients of the Laurent expansion of the transfer function $W(s)$ about the complex point s_i .

Remark 2. The idea of the moment-based model order reduction technique is based on interpolating the transfer function of the original system (and the derivatives of this) and the transfer function of the reduced order model (and the derivatives of this) at these interpolation points s_i .

The pioneering study Astolfi (2010) shows that the moments of a SISO linear system are in a one-to-one relation with the steady-state response (provided it exists) of the output of the interconnection between a signal generator and the system Σ itself. This concept is formally extended to MIMO systems in Faedo et al. (2019) and Peña-Sanchez et al. (2019b), and briefly recalled in the following theorem.

Theorem 1 (Faedo et al., 2019; Peña-Sanchez et al., 2019b). Consider system Eq. 1 and the autonomous multiple-output signal generator

$$\mathcal{G} : \{\dot{\Xi}(t) = (\mathbb{I}_q \otimes S)\Xi(t), u(t) = L\Xi(t)\} \quad (4)$$

with $\Xi(t) \in \mathbb{R}^{qv}$, $S \in \mathbb{R}^{v \times v}$, $L \in \mathbb{R}^{q \times qv}$, $\Xi(0) \in \mathbb{R}^{qv}$, $\lambda(A) \subset \mathbb{C}_{<0}$, $\lambda(S) \subset \mathbb{C}^0$, and the eigenvalues of S are simple. Suppose the triple of matrices $(L, \mathbb{I}_q \otimes S, \Xi(0))$ is minimal. Let $\Pi \in \mathbb{R}^{n \times qv}$ be the (unique) solution of the Sylvester equation

$$A\Pi + BL = \Pi(\mathbb{I}_q \otimes S) \quad (5)$$

Then, there exists a one-to-one relation between the moments $\eta_0(s_1), \eta_0(s_2), \dots, \eta_0(s_r)$, with $s_i \in \lambda(S)$ for all $i \in \mathbb{N}_r$, and the steady-state response $C\Pi\Xi$ of the output y of the interconnection of system Eq. 1 with the signal generator Eq. 4.

Remark 3. The minimality of the triple $(L, \mathbb{I}_q \otimes S, \Xi(0))$ implies the observability of the pair $(L, \mathbb{I}_q \otimes S)$ and the excitability of the pair $(\mathbb{I}_q \otimes S, \Xi(0))$.

Remark 4. From now on, we refer to the matrix $C\Pi \equiv \underline{y}$, with Π the solution of Eq. 5, as the moment-domain equivalent of y .

Following this steady-state interpretation of moments, we now recall from Astolfi (2010) the formal definition of a reduced order model achieving moment-matching for system Eq. 1.

Definition 2 (Astolfi, 2010). Consider system Eq. 1 and the signal generator Eq. 4. The system described by the equations

$$\Sigma_{\mathcal{G}} : \{\dot{\Theta}(t) = F\Theta(t) + Gu(t), \theta(t) = Q\Theta(t)\} \quad (6)$$

with $\Theta \in \mathbb{R}^{qv}$, $\theta(t) \in \mathbb{R}^q$, $F \in \mathbb{R}^{qv \times qv}$, $G \in \mathbb{R}^{qv \times q}$, and $Q \in \mathbb{R}^{q \times qv}$ is a model of system Eq. 1 at S if system Eq. 6 has the same moments at S as system Eq. 1.

Lemma 1 (Astolfi, 2010). Consider system Eq. 1 and the signal generator Eq. 4. Then, the system defined in Eq. 6 is a model of system Eq. 1 at S if $\lambda(F) \cap \lambda(S) = \emptyset$ and

$$\underline{y} = QP \quad (7)$$

where $\underline{y} = C\Pi$ is the moment-domain equivalent of the output of system Eq. 1 computed from Eq. 5, and P is the unique solution of the Sylvester equation

$$FP + GL = P(\mathbb{I}_q \otimes S) \quad (8)$$

Remark 5. The transfer function of system $\Sigma_{\mathcal{F}}$ interpolates the transfer function of system Σ at the eigenvalues of the matrix S . Equivalently, the steady-state output of the reduced order model Eq. 6 exactly matches the steady-state output of the system resulting from the interconnection of systems Eq. 1 and Eq. 4.

Given the characteristics of $\lambda(S)$ in Theorem 1, we set a standing assumption on the matrix S and we recall a useful lemma from Faedo et al. (2019) that provides an alternative path for the computation of the matrix $\underline{y} = C\Pi$ in terms of the impulse response matrix of Σ .

Assumption 1. Consider the finite set $\mathcal{F} = 0 \cup \{\omega_p\}_{p=1}^f \subset \mathbb{R}^+$. The matrix S in Eq. 4 is written in block-diagonal form as

$$S = 0 \oplus \left(\bigoplus_{p=1}^f \begin{bmatrix} 0 & \omega_p \\ -\omega_p & 0 \end{bmatrix} \right) \quad (9)$$

where $\nu = 2f + 1$, $f \geq 0$ integer.

Lemma 2 (Faedo et al., 2019, Peña-Sanchez et al., 2019b). Consider the interconnection between system Eq. 1 and the signal generator Eq. 4, and suppose Assumption 1 holds. Without losing generality, assume that $\Xi(0) = [1 \ \varepsilon_{\nu-1}^T]^T$ so that the minimality of the triple $(L, \mathbb{I}_q \otimes S, \Xi(0))$ holds as long as the pair $(L, \mathbb{I}_q \otimes S)$ is observable. Then, the moment-domain equivalent \underline{y} can be computed from the impulse response of Σ as

$$\underline{y} = \sum_{i=1}^q \sum_{j=1}^q e_{ij}^q L (\mathbb{I}_q \otimes \mathcal{R}_{ij}^w) \quad (10)$$

where each $\mathcal{R}_{ij}^w \in \mathbb{R}^{\nu \times \nu}$ is a block-diagonal matrix defined by

$$\mathcal{R}_{ij}^w = W_{ij}(0) \oplus \left(\bigoplus_{p=1}^f \begin{bmatrix} \Re\{W_{ij}(j\omega_p)\} & \Im\{W_{ij}(j\omega_p)\} \\ -\Im\{W_{ij}(j\omega_p)\} & \Re\{W_{ij}(j\omega_p)\} \end{bmatrix} \right) \quad (11)$$

and $W_{ij}(s) = \mathcal{L}\{w_{ij}(t)\}$.

Remark 6. Note that, following Lemma 2, each ω_p in Eq. 9 represents a desired interpolation point for the model reduction process, i.e., a frequency where the transfer function of system $\Sigma_{\mathcal{F}}$ matches the transfer function of the original system Σ .

Remark 7. The set \mathcal{F} , as defined in this study, inherently incorporates the zero element; i.e., we always consider matching at $s = 0$. This is particularly useful for a proper parameterisation of the radiation force subsystem, as it helps to enforce physical properties (see ‘‘Moment-Based Radiation Systems’’).

EQUATIONS OF MOTION FOR A MULTI-DoF WEC

We now introduce the key concepts behind linear modelling of multi-DoF WECs, both in the time and frequency domains. The assumptions considered herein are consistent across a wide variety of WEC control/estimation studies such as Faedo et al. (2019).

Equations in the Time Domain

The motion for a WEC with N DoF can be expressed in the time domain according to Newton’s second law, obtaining the

following linear hydrodynamic formulation:

$$M\ddot{\chi}(t) = \mathcal{F}_r(t) + \mathcal{F}_h(t) + \mathcal{F}_e(t) \quad (12)$$

where $M = \bigoplus_{i=1}^N m_i$ is the mass matrix of the buoy with $m_i \in \mathbb{R}^+$ the mass of the i th DoF, and the elements of the vectors $\{\chi(t), \mathcal{F}_e(t), \mathcal{F}_h(t), \mathcal{F}_r(t)\} \subset \mathbb{R}^N$ contain the excursion x_i , excitation force f_{e_i} , hydrostatic restoring force f_{h_i} , and radiation force f_{r_i} acting on the i th DoF, with $i \in \mathbb{N}_N$, respectively.

The linearised hydrostatic force \mathcal{F}_h can be written as $-S_h\chi$, where the matrix $S_h \in \mathbb{R}^{N \times N}$ is defined as $S_h = \sum_{i=1}^N \sum_{j=1}^N e_{ij}^N \otimes s_{h_{ij}}$ and contains the hydrostatic stiffness of each DoF (if $i = j$) and each interaction between the different modes of motion of the device due to the movement of each other DoF (if $i \neq j$). The radiation force \mathcal{F}_r is modelled from linear potential theory and, using Cummins’ equation (Cummins, 1962), is

$$\mathcal{F}_r(t) = -\mu_{\infty}\ddot{\chi}(t) - \int_{\mathbb{R}^+} K(\tau)\dot{\chi}(t - \tau) d\tau \quad (13)$$

where $\mu_{\infty} = \lim_{\omega \rightarrow +\infty} A(\omega)$ represents the added-mass matrix at infinite frequency (Falnes, 2002) and $K(t) = \sum_{i=1}^N \sum_{j=1}^N e_{ij}^N \otimes k_{ij}(t) \in \mathbb{R}^{N \times N}$, $k_{ij} \in L^2(\mathbb{R})$ contains the (causal) radiation impulse response of each DoF (if $i = j$) and each interaction due to radiated waves created by the motion of other DoF (if $i \neq j$). Finally, we can express the linearised equation of motion of the multi-DoF WEC as

$$(M + \mu_{\infty})\ddot{\chi}(t) + K(t) * \dot{\chi}(t) + S_h\chi(t) = \mathcal{F}_e(t) \quad (14)$$

Equations in the Frequency Domain

Applying the Fourier transform to Eq. 14 and considering the velocity of each DoF a measurable output (i.e., $\dot{\chi}(t)$), the following representation

$$\hat{\chi}(j\omega) = \hat{\mathcal{F}}_e(j\omega)H(j\omega) \quad (15)$$

where $H : \mathbb{C}^0 \rightarrow \mathbb{C}^{N \times N}$ denotes the force-to-velocity frequency response mapping of the WEC, holds. The response $H(j\omega)$ can be readily computed (Falnes, 2002) as

$$H(j\omega) = \left(B(\omega) + j\omega(A(\omega) + M) + \frac{S_h}{j\omega} \right)^{-1} \quad (16)$$

where $B(\omega)$ and $A(\omega)$ represent the radiation damping and the radiation added mass matrix of the device, respectively. These parameters are calculated using hydrodynamic codes at a finite set of uniformly spaced frequency samples $\Omega = \{\omega_i\}_{i=1}^M$ with $\Omega \subset [\omega_l, \omega_u]$, where ω_l and ω_u represent the lower and upper bounds of the range, respectively. We note that the ideal frequency range depends explicitly on the application, as discussed in Faedo et al. (2018b).

Mapping Between Time and Frequency

Following the study performed in Ogilvie (1964), we recall that there exists a straightforward relation between the parameters of the models Eq. 14 and Eq. 15, which can be readily obtained via a direct application of the Fourier transform as

$$B(\omega) = \int_{\mathbb{R}^+} K(t) \cos(\omega t) dt, \quad (17)$$

$$A(\omega) = \mu_{\infty} - \frac{1}{\omega} \int_{\mathbb{R}^+} K(t) \sin(\omega t) dt$$

Property	Significance on K
(I) $\lim_{\omega \rightarrow +\infty} K(j\omega) = 0$	Strictly proper
(II) $\lim_{t \rightarrow +\infty} K(t) = 0$	BIBO stable
(III) $\lim_{\omega \rightarrow 0} K(j\omega) = 0$	With transmission zeros at the origin
(IV) $\Re\{K_{ii}(j\omega)\} > 0, \forall i \in \mathbb{N}_N$	Passivity (see Khalil, 1996, for a proof).

Table 1 Properties of the radiation kernel K

Then, the radiation force impulse response mapping $K : \mathbb{R}^+ \rightarrow \mathbb{R}^{N \times N}$ can be directly written (Falnes, 2002) as

$$K(t) = \frac{2}{\pi} \int_{\mathbb{R}^+} B(\omega) \cos(\omega t) d\omega \quad (18)$$

Considering Eq. 18, the frequency-domain representation of the radiation force kernel K can be obtained as

$$K(j\omega) = B(\omega) + j\omega[A(\omega) - \mu_\infty] \quad (19)$$

The radiation kernel frequency response $K(j\omega)$ has a set of particular properties that have been used in the literature to enforce a structure on the parametric model used to identify the frequency-domain data. Such properties are recalled in Table 1.

MOMENT-BASED RADIATION SYSTEM

The radiation impulse response mapping defines a linear-time invariant system completely characterised by $K : \mathbb{R}^+ \rightarrow \mathbb{R}^{N \times N}$, where its input is the vector containing the device velocities for each DoF, i.e., $\dot{\chi}$. To be precise, the radiation subsystem Σ^K is given by

$$\Sigma_K : \theta_K(t) = K(t) * \dot{\chi}(t) \quad (20)$$

where $\theta_K(t) \in \mathbb{R}^N$ is the output (radiation force) of system Σ_K .

With the definition of Σ_K , and following the theory presented in ‘‘Moments for MIMO Systems,’’ we can obtain a parametric model $\tilde{\Sigma}_{K\mathcal{F}}$ for the radiation force subsystem defined in Eq. 20 using the result of Lemma 2, which offers an explicit computation of the moment-domain equivalent of a system in terms of its impulse response mapping. To that end, and in the spirit of Assumption 1, we express the velocity of the multi-DoF WEC $\dot{\chi}$ as an autonomous multiple-output signal generator in a similar fashion to \mathcal{G} in Eq. 4, i.e.,

$$\mathcal{G}_{\dot{\chi}} : \{\dot{\Xi}_{\dot{\chi}}(t) = (\mathbb{I}_N \otimes S) \Xi_{\dot{\chi}}(t), \dot{\chi}(t) = L_{\dot{\chi}} \Xi_{\dot{\chi}}(t)\} \quad (21)$$

with S as in Eq. 9, $\dot{\Xi}_{\dot{\chi}}(0) = [1 \ \epsilon_{\nu-1}^T]^T$ and $L_{\dot{\chi}}$ such that the pair $(L_{\dot{\chi}}, S)$ is observable. Then, recalling the result of Lemma 2, the moment-domain equivalent of the output of system Σ_K in Eq. 20 can be straightforwardly computed as

$$\underline{y}_K = \sum_{i=1}^N \sum_{j=1}^N e_{ij}^N L_{\dot{\chi}} (\mathbb{I}_N \otimes \mathcal{R}_{ij}^k) \quad (22)$$

where each $\mathcal{R}_{ij}^k \in \mathbb{R}^{\nu \times \nu}$ is a block-diagonal matrix defined by

$$\mathcal{R}_{ij}^k = 0 \oplus \left(\bigoplus_{p=1}^f \begin{bmatrix} \Re\{K_{ij}(j\omega_p)\} & \Im\{K_{ij}(j\omega_p)\} \\ -\Im\{K_{ij}(j\omega_p)\} & \Re\{K_{ij}(j\omega_p)\} \end{bmatrix} \right) \quad (23)$$

Note that each entry of \mathcal{R}_{ij}^k directly depends on the hydrodynamic coefficients computed with BEM solvers. To be precise, let $A_{ij}(\omega)$ and $B_{ij}(\omega)$ be the ij th element of the added mass matrix $A(\omega)$

and the radiation damping matrix $B(\omega)$ of the device, respectively. Then,

$$\begin{aligned} \Re\{K_{ij}(j\omega_p)\} &= B_{ij}(\omega_p), \\ \Im\{K_{ij}(j\omega_p)\} &= \omega_p[A_{ij}(\omega_p) - \mu_{\infty ij}] \end{aligned} \quad (24)$$

where $\mu_{\infty ij}$ is the ij -th element of the matrix μ_∞ .

Remark 8. Note that each matrix \mathcal{R}_{ij}^k already incorporates the hydrodynamic property $K_{ij}(0) = 0$ (see Table 1, Property III).

Finally, following Definition 2 and Lemma 1, we note that the parametric (state-space) description

$$\tilde{\Sigma}_{K\mathcal{F}} : \{\dot{\Theta}_K(t) = F_K \Theta_K(t) + G_K \chi(t), \tilde{\theta}_K(t) = Q_K \Theta_K(t)\} \quad (25)$$

is a system that interpolates the target frequency response $K(j\omega)$ at the set \mathcal{F} ; i.e., it has the exact same frequency response of the radiation subsystem Σ_K at the frequencies defined in the set \mathcal{F} , if $Q_K P_K = \underline{y}_K$, where $P_K \in \mathbb{R}^{\nu \times \nu}$ is the unique solution of the Sylvester equation

$$F_K P_K + G_K L_{\dot{\chi}} = P_K (\mathbb{I}_N \otimes S) \quad (26)$$

and \underline{y}_K is computed from Eq. 22. The explicit computation of the matrices F_K, G_K, Q_K in Eq. 25 (fulfilling condition Eq. 26) is addressed in the following section.

MODELS ACHIEVING MOMENT-MATCHING

Herein, we briefly summarise some of the key concepts behind the algorithm proposed in Peña-Sanchez et al. (2019b) to compute a moment-based time-domain model for an array of WECs, and we adapt the procedure for our multi-DoF radiation force subsystem case. We note that Peña-Sanchez et al. (2019b) regard the moment-based concepts described in this study in synergy with well-known results of subspace-based identification methods, as detailed in McKelvey et al. (1996).

To be precise, we approximate the dynamic and output matrix from the target radiation subsystem Σ_K in terms of the corresponding singular value decomposition of the Hankel matrix \mathcal{H} (see McKelvey et al., 1996), constructed from $K(j\omega)$ as defined in Eq. 19 and computed at the finite set of uniformly spaced frequencies Ω (see ‘‘Equations of Motion for a Multi-DoF WEC’’). These α -dimensional approximated matrices ${}^d\hat{A}_\alpha \in \mathbb{R}^{\alpha \times \alpha}$, $\hat{C}_\alpha \in \mathbb{R}^{N \times \alpha}$ (where ${}^d\hat{A}_\alpha$ corresponds to a discrete-time model) can be computed as

$${}^d\hat{A}_\alpha = (J_1 \hat{U}_\alpha)^\dagger J_2 \hat{U}_\alpha, \quad \hat{C}_\alpha = J_3 \hat{U}_\alpha \quad (27)$$

where the continuous-time equivalent matrix \hat{A}_α can be obtained directly from ${}^d\hat{A}_\alpha$ using, for instance, the bilinear transformation. We refer the reader to McKelvey et al. (1996) for the explicit expression of the matrices J_1, J_2, J_3 , and \hat{U}_α .

Remark 9. If ${}^d\hat{A}_\alpha$, computed as in Eq. 27, has unstable eigenvalues, one can always project such a set into the complex unit circle following the procedure described in McKelvey et al. (1996).

Finally, the moment-based identification algorithm for the radiation force subsystem utilised herein can be summarised in the following steps:

- I Select a set of f interpolation points (frequencies ω_p) $\mathcal{F} = 0 \cup \{\omega_p\}_{p=1}^f$ to achieve moment-matching.

- II Compute the matrix $\mathbb{1}_N \otimes S$ following Eq. 9 and select any $L_{\dot{\chi}}$ such that the pair $(L_{\dot{\chi}}, \mathbb{1}_N \otimes S)$ is observable.
- III Calculate the moment-domain equivalent of the output of system Eq. 20 \underline{y}_K using Equation 22.
- IV Compute the matrices $\hat{A}_{N\nu}$ and $\hat{C}_{N\nu}$ from Eq. 27 (We note that standard MATLAB routines can be used to obtain $\hat{A}_{N\nu}$ and $\hat{C}_{N\nu}$ from the frequency-domain data $K(j\omega)$).
- V Consider the parametric model for the radiation subsystem described in Eq. 25 and set $F_K = \hat{A}_{N\nu}$ and $Q_K = \hat{C}_{N\nu}$.
- VI Consider the frequency response of Eq. 25, i.e.,

$$\tilde{K}(j\omega, G_K) = Q_K(j\omega_i - F_K)^{-1} G_K.$$

Using the frequency set $\Omega = \{\omega_i\}_{i=1}^M$, compute the input matrix G_K^{opt} with the following optimisation-based procedure:

$$G_K^{\text{opt}} = \arg \min_{G_K} \sum_{i=1}^M \|\tilde{K}(j\omega_i, G_K) - K(j\omega_i)\|_F^2$$

subject to

$$F_K P_K + G_K L_{\dot{\chi}} = P_K (\mathbb{1}_N \otimes S), \quad Q_K P_K = \underline{y}_K.$$

- VII Compute a $N\nu$ -dimensional radiation force subsystem time-domain model $\tilde{\Sigma}_{K\mathcal{F}}$ achieving moment-matching at S as

$$\tilde{\Sigma}_{K\mathcal{F}} : \{\dot{\Theta}_K(t) = F_K \Theta_K(t) + G_K^{\text{opt}} \dot{\chi}(t), \quad \tilde{\theta}_K(t) = Q_K \Theta_K(t)\}.$$

Remark 10. The method is based on the idea of building the model $\tilde{\Sigma}_{K\mathcal{F}}$ by matching the $f + 1$ (user-defined) frequencies of the set \mathcal{F} , exploiting the system structure of Eq. 25, and solving for an equality-constrained optimisation problem, which computes the input matrix G_K^{opt} that minimises the difference between the target frequency response and that of Eq. 25, while ensuring the moment-matching conditions in the model.

APPLICATION TO A CORPOWER-LIKE DEVICE

To illustrate the strategy proposed in this study, we consider the CorPower-like device utilised in Giorgi and Ringwood (2019) (note that the applicability of the method is independent of the specific device geometry) and depicted here in Fig. 1a. We refer the reader to Giorgi and Ringwood (2019) for a precise description of the dimensions of this device.

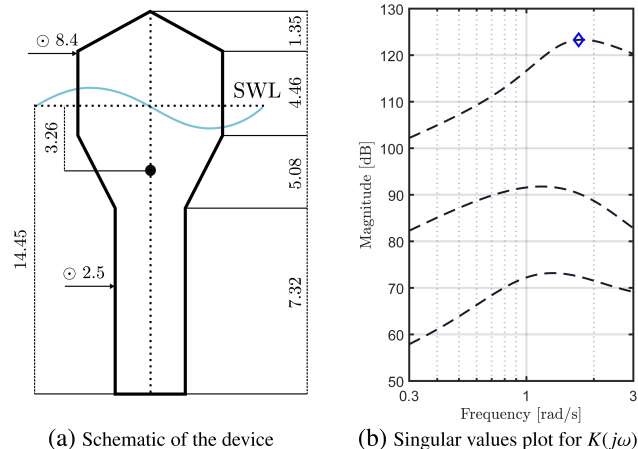


Fig. 1 CorPower-like device considered in this study; SWL, still water level

Following the analysis carried out in Giorgi and Ringwood (2019), we consider surge (mode 1), heave (mode 2), and pitch (mode 3) as the more relevant DoF for this particular application case. The corresponding hydrodynamic parameters $A(\omega)$ and $B(\omega)$ can be appreciated in Fig. 2. Note that the elements $\{1, 2\}$, $\{2, 1\}$, $\{2, 3\}$, $\{3, 2\}$ of the matrices $A(\omega)$ and $B(\omega)$ are not shown in Fig. 2, given that there is no interaction due to radiation forces between these particular modes of motions; i.e., they are exactly zero for all $\omega \in \mathbb{R}^+$. The maximum frequency selected in the BEM code, to compute the hydrodynamic parameters of the CorPower-like device of Fig. 2, is set to 10 rad/s. Nevertheless, we note that ocean waves peak periods typically lie between 3 s and 16 s, which implies that the frequency range of the wave excitation force \mathcal{F}_e is approximately $[0.4, 2.1]$ rad/s (Faedo et al., 2018b). Hence, it is straightforward to conclude that, under the modelling assumptions considered in “Equations of Motion for a Multi-DoF WEC,” the velocity of the multi-DoF device (input to Σ_K) has significant frequency components in the same range.

From now on, we denote the frequency-domain model of the radiation subsystem corresponding to our CorPower-like device $K(j\omega)$ as the target response. In addition, we use the notation $K_{ij}(j\omega)$ for the ij element of the matrix $K(j\omega)$. More precisely, $K_{ij} : \mathbb{C}^0 \rightarrow \mathbb{C}$ is the frequency response mapping between the output i (radiation force exerted on the i th mode) and the input j (velocity of the j th mode).

Approximation of the Radiation Subsystem

We now specifically proceed with the computation of a moment-based approximation $\tilde{\Sigma}_{K\mathcal{F}}$ for the radiation subsystem Σ_K , based on the knowledge of the target frequency response $K(j\omega)$ and using the procedure described in “Models Achieving Moment-Matching.”

Recall that the first step of the algorithm is to select the set of frequencies \mathcal{F} to interpolate. In the SISO case (1-DoF device) of Faedo et al. (2018b), a sensible choice can be made by analysing the gain of $K(j\omega)$, and selecting dynamically important points, such as the resonant frequency of the particular DoF under study, i.e., where the maximum amplification occurs. For this MIMO case, it is well-known that the system gain depends on the corresponding input direction (see, for example, Zhou and Doyle, 1998), so that this set of dynamically important points cannot be obtained by inspecting each element $K_{ij}(j\omega)$ independently. Instead, we use the singular values of $K(j\omega)$ (Zhou and Doyle, 1998), which are plotted in Fig. 1b.

Following well-known theory for MIMO systems, it is straightforward to notice, from Fig. 1b, that $\omega \approx 1.7$ rad/s represents an interpolation point of dynamical importance (marked with a blue diamond in Fig. 1b), being the frequency where the maximum amplification occurs, i.e., the frequency characterising the \mathcal{H}_∞ -norm of the system (Zhou and Doyle, 1998).

Based on this, we propose two different frequency interpolation sets \mathcal{F} , as follows:

$$\mathcal{F}_1 = \{0, 1.7\}, \quad \mathcal{F}_2 = \{0, 0.8, 1.7\}$$

where \mathcal{F}_2 includes the set \mathcal{F}_1 and incorporates an additional low frequency component $\omega = 0.8$ rad/s. Note that both sets include the zero element (see Remark 7). Following the discussion provided at the beginning of this section, the frequency range selected to approximate $K(j\omega)$ is given by $\Omega = [0.3, 3]$ rad/s, with a frequency discretisation step of 0.01 rad/s. Given that heave (mode 2) is the main DoF of this WEC, Fig. 3 presents the Bode diagram for the target response $K_{22}(j\omega)$ (dashed black) and the

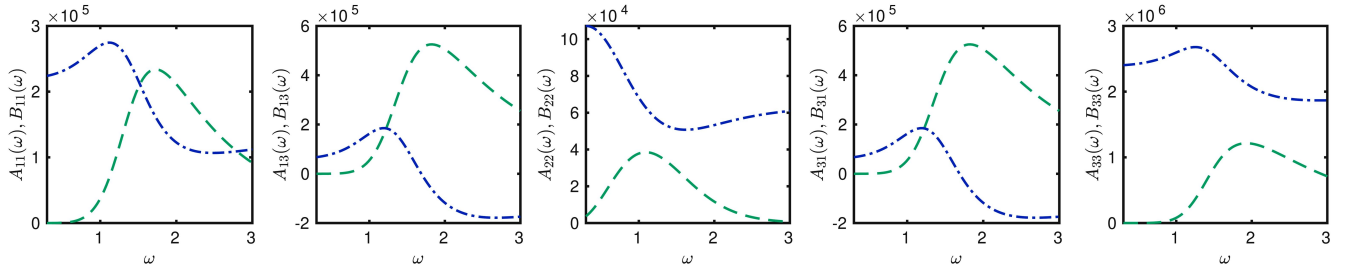


Fig. 2 Hydrodynamic parameters $A(\omega)$ (dot-dashed blue) and $B(\omega)$ (dashed green) for the CorPower-like device considered herein

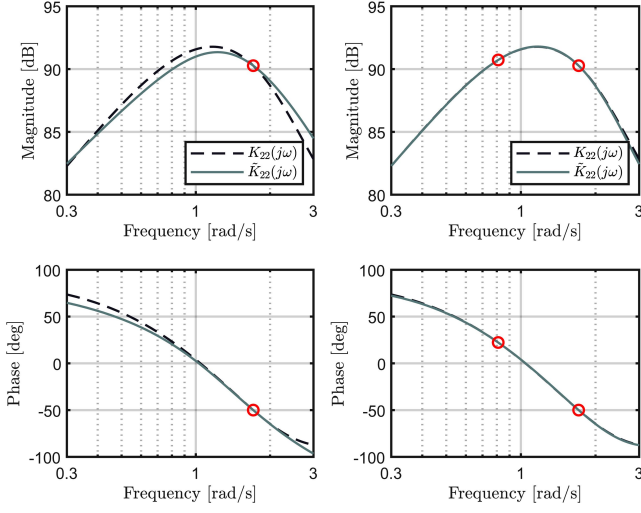


Fig. 3 Bode diagram for $K_{22}(j\omega)$ (dashed black), and $\tilde{K}_{22}(j\omega)$ (solid gray) for both parametric models $\tilde{\Sigma}_{K\mathcal{F}_1}$ (left) and $\tilde{\Sigma}_{K\mathcal{F}_2}$ (right), with interpolation points (empty red circles)

moment-based approximated response $\tilde{K}_{22}(j\omega)$ (solid gray) for both parametric models $\tilde{\Sigma}_{K\mathcal{F}_1}$ (left) and $\tilde{\Sigma}_{K\mathcal{F}_2}$ (right). The interpolation points for each model are denoted by an empty red circle. As expected, the approximated systems have the exact same frequency response as the target model for each corresponding set \mathcal{F} . Though using the set \mathcal{F}_1 as the interpolation set provides quite accurate results, the decrease in the approximation error from system $\tilde{\Sigma}_{K\mathcal{F}_1}$ to $\tilde{\Sigma}_{K\mathcal{F}_2}$ can be clearly appreciated.

As a conclusive graphical illustration of the frequency-domain performance for the models computed via our strategy, Fig. 4 presents the singular value plot for the target response $K(j\omega)$, and the approximated mapping $\tilde{K}(j\omega)$, both for $\tilde{\Sigma}_{K\mathcal{F}_1}$ (left) and $\tilde{\Sigma}_{K\mathcal{F}_2}$ (right). It can be readily appreciated that both models can accurately approximate the target singular values in every principal direction (i.e., the target MIMO gain) with an increase in accuracy when using the interpolation set \mathcal{F}_2 instead of \mathcal{F}_1 .

Aiming to further assess the strategy, Table 2 offers a numerical appraisal of each of the moment-matching-based parametric models in terms of the following parameters:

Dim: Dimension (order) of the parametric model

NRMSE_F: Normalized Root-Mean-Square Error (NRMSE) computed against the target WEC frequency response $\forall \omega \in \Omega$.

NRMSE_T: NRMSE computed (in steady-state) against the target steady-state radiation system response using inputs generated with frequency content inside the set Ω .

In order to get meaningful results for the time-domain scenario of Table 2, and since the inputs are generated from sets of random amplitudes, it is found that the mean of 10 simulations is

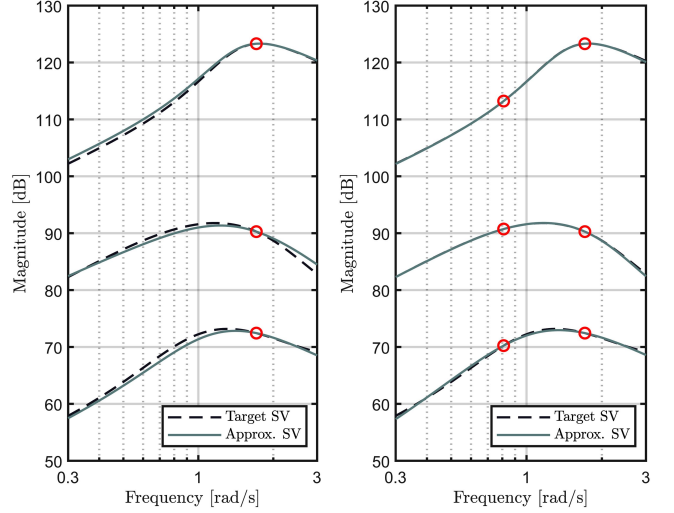


Fig. 4 Singular value (SV) plot for $K(j\omega)$ (dashed black) and $\tilde{K}(j\omega)$ (solid gray), with interpolation points (empty red circles)

necessary to obtain a 95% confidence interval with a half-width of 0.25% of the mean, computed as in Peña-Sánchez et al. (2018).

The first row of Table 2 includes the “multi-SISO,” which corresponds to a parametric model of the MIMO system Σ_K obtained by approximating each individual element of the matrix $K(j\omega)$ with a SISO system. Though several strategies can be used to obtain this “multi-SISO” system, we select herein the SISO moment-matching method described in Faedo et al. (2018b) (with \mathcal{F}_2 as interpolation points), resulting in a model of dimension 25. This is merely motivated by the comparison study (Peña-Sánchez et al., 2019a), where the SISO moment-matching method is shown to outperform well-established strategies, both in terms of performance and preservation of physical characteristics.

As can be appreciated in Table 2, note that the approach proposed herein provides highly accurate results even with a single interpolation point (in addition to the zero frequency), with only approximately 4% of error in both the frequency domain and time domain, and with an intrinsic decrease in computational complexity, given the low dimension (order) of the resulting model. We also note that the “multi-SISO” approach provides similar results to those of $\tilde{\Sigma}_{K\mathcal{F}_2}$ with higher computational requirements (i.e.,

Model	Dim	NRMSE _F	NRMSE _T
“multi-SISO”	28	1.036%	0.985%
$\tilde{\Sigma}_{K\mathcal{F}_1}$	9	3.580%	4.045%
$\tilde{\Sigma}_{K\mathcal{F}_2}$	15	1.092%	0.664%

Table 2 Numerical comparison table

higher system order). That said, we emphasize that the radiation subsystem should be treated as a MIMO system when it comes to its parametric approximation.

To conclude the assessment of our strategy, we analyse the moment-based computed models $\tilde{\Sigma}_{K\mathcal{F}}$ with respect to the physical properties of the radiation subsystem listed in Table 1.

- *Property I* (Σ_K is strictly proper): This property is always fulfilled by the family of parametric models defined in Eq. 25. See, for example, Khalil (1996).

- *Property II* (Σ_K is BIBO stable): The strategy proposed in “Models Achieving Moment-Matching” preserves the dynamic matrix approximated by using the Hankel matrix associated with $K(j\omega)$. This matrix can always be constructed so that it is Hurwitz (see Remark 10), and, hence, system $\tilde{\Sigma}_{K\mathcal{F}}$ is BIBO stable. By way of example, Fig. 5 shows the pole-zero map for system $\tilde{\Sigma}_{K\mathcal{F}_1}$ computed in this same section for the CorPower-like device. It can be appreciated that all the poles are contained in the open left-half of the complex plane; i.e., $\tilde{\Sigma}_{K\mathcal{F}_1}$ is BIBO stable.

- *Property III* (Σ_K has transmission zeros at $s = 0$): This property is specifically enforced by considering 0 as part of the set of interpolation points \mathcal{F} (see Remark 8). In practice, this can be (graphically) appreciated in the pole-zero map of Fig. 5, where the zero at $s = 0$ manifests explicitly for the approximating model $\tilde{\Sigma}_{K\mathcal{F}_1}$.

- *Property IV* (Σ_K is passive): This particular physical property is not enforced by our strategy. However, we note that, if the target data $K(j\omega)$ effectively come from a passive model, the parametric models computed with our strategy, for the WEC radiation force subsystem, are virtually inherently passive. If required by the application, a similar strategy to that of Faedo et al. (2018a) can

be considered to specifically ensure passivity within this multi-DoF moment-based framework. Figure 6 depicts the Nyquist plot for the diagonal elements of $\tilde{K}(j\omega)$ for $\tilde{\Sigma}_{K\mathcal{F}_2}$, where it can be appreciated that $\Re\{\tilde{K}_{ii}(j\omega)\} > 0$ for all $i \in \mathbb{N}_3$ and, hence, $\Sigma_{K\mathcal{F}_2}$ is passive.

CONCLUSIONS

This paper presents a MIMO moment-based identification framework for the radiation force subsystem of multi-DoF WECs. The proposed strategy computes a parametric model of the target radiation force mapping using raw frequency-domain data produced by well-known BEM-based hydrodynamic codes. Such a moment-based model exactly matches the target steady-state response for a user-defined set of frequencies, allowing for the preservation of the relevant dynamic characteristics of the device. Moreover, we show that this parametric approximation retains important properties of radiation forces, such as input-output stability and passivity, agreeing with the underlying physics that characterise such a system. The performance of the strategy is demonstrated and analysed from both a time- and a frequency-domain perspective, using a CorPower-like multi-DoF device as application case.

ACKNOWLEDGEMENTS

The authors thank Prof. Alessandro Astolfi and Dr. Giordano Scarciotti from Imperial College London, for useful discussions on moments. This material is based upon works supported by Science Foundation Ireland under Grant no. 13/IA/1886.

REFERENCES

Astolfi, A (2010). “Model Reduction by Moment Matching for Linear and Nonlinear Systems,” *IEEE Trans Automat Control*, 55(10), 2321–2336. <https://doi.org/10.1109/TAC.2010.2046044>.

Cummins, WE (1962). “The Impulse Response Function and Ship Motions,” *Schiffstechnik*, 47, 101–109.

Faedo, N, Olaya, S, and Ringwood, JV (2017). “Optimal Control, MPC and MPC-Like Algorithms for Wave Energy Systems: An Overview,” *IFAC J Syst Control*, 1, 37–56. <https://doi.org/10.1016/j.ifacsc.2017.07.001>.

Faedo, N, Peña-Sanchez, Y, and Ringwood, JV (2018a). “Passivity Preserving Moment-Based Finite-Order Hydrodynamic Model Identification for Wave Energy Applications,” In *Advances in Renewable Energies Offshore, RENEW 2018*, 351–359.

Faedo, N, Peña-Sanchez, Y, and Ringwood, JV (2018b). “Finite-Order Hydrodynamic Model Determination for Wave Energy Applications Using Moment-Matching,” *Ocean Eng*, 163, 251–263. <https://doi.org/10.1016/j.oceaneng.2018.05.037>.

Faedo, N, Scarciotti, G, Astolfi, A, and Ringwood, JV (2019). “Moment-Based Constrained Optimal Control of an Array of Wave Energy Converters,” In *American Control Conference (ACC)*, Philadelphia, PA, USA, 4797–4802.

Falnes, J (2002). *Ocean Waves and Oscillating Systems: Linear Interactions Including Wave-Energy Extraction*, Cambridge University Press, Cambridge, UK, 275 pp.

Giorgi, G, and Ringwood, JV (2019). “A Compact 6-DoF Nonlinear Wave Energy Device Model for Power Assessment and Control Investigations,” *IEEE Trans Sustain Energy*, 10(1), 119–126. <https://doi.org/10.1109/TSTE.2018.2826578>.

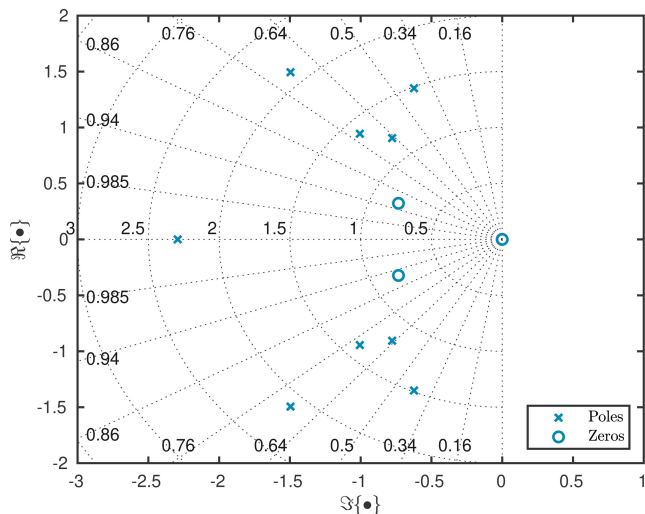


Fig. 5 Pole-zero map for the approximating model $\tilde{\Sigma}_{K\mathcal{F}_1}$

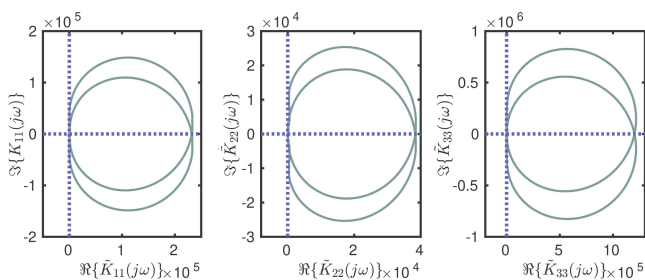


Fig. 6 Nyquist plot (diagonal elements) of $\tilde{K}(j\omega)$ for $\tilde{\Sigma}_{K\mathcal{F}_2}$

- Khalil, HK (1996). *Nonlinear Systems*, Prentice-Hall, 734 pp.
- Li, Y, and Yu, Y-H (2012). "A Synthesis of Numerical Methods for Modeling Wave Energy Converter-Point Absorbers," *Renewable Sustainable Energy Rev*, 16(6), 4352–4364. <https://doi.org/10.1016/j.rser.2011.11.008>.
- McKelvey, T, Akçay, H, and Ljung, L (1996). "Subspace-Based Multivariable System Identification from Frequency Response Data," *IEEE Trans Automatic Control*, 41(7), 960–979. <https://doi.org/10.1109/9.508900>.
- Ogilvie, TF (1964). "Recent Progress Toward the Understanding and Prediction of Ship Motions," *5th Symp Naval Hydrodyn*, Bergen, Norway, 3–80.
- Peña-Sanchez, Y, Faedo, N, and Ringwood, JV (2019a). "A Critical Comparison Between Parametric Approximation Methods for Radiation Forces in Wave Energy Systems," *Proc 29th Int Ocean Polar Eng Conf*, Honolulu, HI, USA, ISOPE, 1, 174–181.
- Peña-Sanchez, Y, Faedo, N, and Ringwood, JV (2019b). "Moment-Based Parametric Identification of Arrays of Wave Energy Converters," *Am Control Conf (ACC)*, Philadelphia, PA, USA, 4785–4790.
- Peña-Sanchez, Y, Garcia-Abril, M, Paparella, F, and Ringwood, JV (2018). "Estimation and Forecasting of Excitation Force for Arrays of Wave Energy Devices," *IEEE Trans Sustainable Energy*, 9(4), 1672–1680. <https://doi.org/10.1109/TSTE.2018.2807880>.
- Penalba, M, Kelly, T, and Ringwood, JV (2017). "Using NEMOH for Modelling Wave Energy Converters: A Comparative Study with WAMIT," *Proc 12th Eur Wave Tidal Energy Conf*, Cork, Ireland, 631.
- Pérez, T, and Fossen, T (2008). "Joint Identification of Infinite-Frequency Added Mass and Fluid-Memory Models of Marine Structures," *Model Identif Control*, 29(3), 93–102. <https://doi.org/10.4173/mic.2008.3.2>.
- Scarciotti, G, and Astolfi, A (2017). "Nonlinear Model Reduction by Moment Matching," *Foundations Trends Syst Control*, 4(3-4), 224–409. <https://doi.org/10.1561/26000000012>.
- Zhou, K, and Doyle, JC (1998). *Essentials of Robust Control*, Volume 104, Prentice-Hall, 411 pp.

**Proceedings of the 14th (2020) ISOPE Pacific/Asia
Offshore Mechanics Symposium (PACOMS-2020 Dalian)**

Dalian, China (Online/Virtual), November 22–25, 2020

**Hydrodynamics Waves CFD Coastal Dynamics Flow-Induced Vibrations
Offshore & Ocean Technology Pipeline Seabed Offshore Wind Turbine
Wave Energy Converters Arctic Ice Technology Surface
Underwater Damage Risk**

The Proceedings (ISBN 978-1-880653-83-8; ISSN 1946-004x), 530 pp: \$100 (ISOPE Member; \$80) in a single volume (USB) available from www.isopec.org (orders@isopec.org), ISOPE, 495 North Whisman Road, Suite 300, Mountain View, CA 94043, USA (Fax+1-650-254-2038)